Numerical study of autoionizing states in completely correlated two-electron systems

S. L. Haan,* R. Grobe, and J. H. Eberly
Department of Physics and Astronomy, University of Rochester, Rochester, New York 14627
(Received 27 September 1993)

The structure of a one-dimensional two-electron model atom analogous to helium is examined. Predictions of Hartree-Fock and basis-state diagonalization methods are compared with results of exact numerical techniques. Particular attention is given to the lowest-energy autoionizing resonance and to how the autoionizing state can be defined. The dynamics of the autoionizing decay are examined with regard to the time development of the spatial wave function and various population amplitudes. The photoabsorption line shape of the lowest-lying autoionizing state for dipole excitation from the first excited state is also presented.

PACS number(s): 32.80.Dz, 32.80.Fb, 31.20.Di, 31.15.+q

I. INTRODUCTION

Multielectron atoms undergoing very strong interactions that lead to rapid ionization present difficult questions in atomic theory. Whether the interaction is radiative or collisional or something else, the ionization process must involve very high-lying atomic states, possibly including a wide variety of multielectron continuum states. It is well known that the accurate description of these states is largely an unsolved problem.

We are particularly concerned with the description of ionizing interactions brought about by laser excitation, which almost automatically means high-order theory is required because several to many laser photons are typically required for ionization. For instance, ionization by Nd:YAG or Nd:YLF lasers requires ten or more photons to reach the first threshold of any of the noble gases (to take common examples). However, not only are there no satisfactory techniques for pursuing high-order multielectron perturbation theory, what is worse is that perturbative results could not even be expected to converge, given the high laser intensities at which multiphoton ionization experiments are now carried out (around 10^{13} W/cm^2 or higher). This means that the $(n+2)$nd-order contribution to a matrix element can be expected to be larger, not smaller, than the nth-order contribution, effectively preventing any sensible theoretical predictions at all through perturbation theory.

The high laser intensity that makes high-order processes both experimentally important and theoretically inaccessible by standard means also provides a justification for at least two nonperturbative approximation methods. If the photon frequency is sufficiently low, the ionization process is almost the same as in a static field. This leads to an approach associated with Keldysh [1] who first suggested it almost 30 years ago. It has been further developed and has provided formulas for ionization rates [2] that are in reasonable agreement with recent experiments on a range of atomic species [3]. In these cases the Keldysh approach is an extension of quantum tunneling theory [1].

An alternative approach, designed for higher-frequency processes in which tunneling approximations cannot be applied, involves deriving an atomic wave function in a direct *ab initio* fashion by numerical solution of the atomic Schrödinger equation on a spatial grid. However, computational resources are still too limited to permit this method to be applied even to the two electrons in He or its isoelectronic partners without some restriction. We will adopt the restriction that the electrons move along only one axis. The atom that results from this restriction to one dimension is only a shadow of real helium, of course, and cannot be expected to substitute for helium in any respect that involves more than one dimension—all questions regarding angular momentum, angular correlations, light polarization other than linear, etc., are out of range. However, the one-dimensional (1D) model appears to have some relevance in regard to questions of purely dynamical behavior—for example, questions regarding single-photon or multiphoton transition rates, power-dependent scaling relations, resonant absorption, ionization, radiated power in the dipole limit, harmonics in light scattering, level occupation probabilities for both bound and free electrons, etc.

If the laser is linearly polarized, we can be more confident of the relevance of a one-dimensional approximation as the laser intensity becomes higher, because the main effect of a strong linearly polarized electric field is to cause linear motion of the electrons along the polarization axis. Experience with 1D calculations in the case of one-electron atoms [4], where comparisons with existing three-dimensional (3D) calculations [5] can be made, gives further evidence that one-dimensional model calculations are not seriously misleading (indeed, can be semiquantitatively correct) in a wide variety of physical situations involving strong laser excitation where alternative approaches are unavailable.

In this paper we will extend two-electron work already reported [6,7] that dealt with a 1D negative ion, an ana-

*Permanent address: Department of Physics and Astronomy, Calvin College, Grand Rapids, MI 49546.

 ©1994 The American Physical Society

log of H^-. We will use the same H^- model but increase the nuclear charge from $Z=1$ to $Z=2$ to obtain the corresponding helium analog. Just as in the real 3D world this simple change has a profound effect. To take the most prominent example, the 1D negative ion was found to have only a single bound level, but the 1D version of helium has a sequence of Rydberg levels below the first ionization threshold. The results reported here are divided into two categories. In Secs. II and III we derive static features of the atom in several ways. We present both eigenenergies and wave functions using exact numerical techniques, Hartree-Fock methods, and basis-state diagonalization. Examples are given for both bound and autoionizing resonance states. We consider in detail the dynamical behavior of the lowest-lying autoionizing resonance. In Sec. IV we consider various dipole matrix elements within the model atom and make connection with the well-known work of Fano [8] concerning autoionizing states. Finally, in Sec. V we provide an overview and summary. We defer investigations of the system's dynamics in the presence of external laser fields to subsequent publications.

II. STATIC FEATURES OF THE TWO-ELECTRON SYSTEM: EXACT AND HARTREE-FOCK METHODS

We consider a system in which two electrons and a fixed nucleus of charge Z interact through a screened Coulomb potential, which was introduced in previous studies [4,6,7]. The Hamiltonian for the system can be written

$$H(x_1,x_2)=\frac{p_1^2}{2}+\frac{p_2^2}{2}+V(x_1,x_2)\ , \tag{1}$$

where

$$V(x_1,x_2)=-\frac{Z}{\sqrt{1+x_1^2}}-\frac{Z}{\sqrt{1+x_2^2}}+\frac{1}{\sqrt{1+(x_1-x_2)^2}}\ . \tag{2}$$

The Hamiltonian describing two electrons in one dimension can also be interpreted as describing a single fictitious particle which moves two dimensions and interacts via the screened Coulomb potential with line charges on each of the axes and along the diagonal $x_2=x_1$. Correspondingly, a two-particle spatial wave function $\Psi(x_1,x_2)$ describing the system is mathematically similar to a wave function describing one particle in two dimensions. Differences occur in physical interpretation and possibly in symmetrization—because of the indistinguishability of the electrons, the two-electron wave function must always satisfy $\Psi(x_1,x_2)=\pm\Psi(x_2,x_1)$. In the absence of orbital motion there is no spin-orbital coupling, so all spin quantum numbers remain conserved. Throughout this work we shall assume the electron spins to be antiparallel, so that the spatial wave function must be symmetric with respect to exchange of the electrons: $\Psi(x_1,x_2)=+\Psi(x_2,x_1)$.

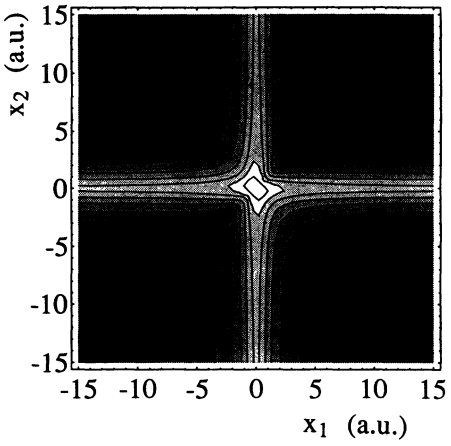

FIG. 1. Contour plot of the potential of Eq. (2) for $Z=2$. In this plot the shading darkens with increasing height.

A contour plot of the potential $V(x_1,x_2)$ of Eq. (2) appears in Fig. 1. The ridge along $x_2=x_1$ which arises from the electron-electron repulsion is clearly visible. Since the lines $x_2=x_1$ and $x_2=-x_1$ are both lines of symmetry for the potential, all nondegenerate eigenfunctions of H must satisfy the condition $\Psi(x_1,x_2)=\pm\Psi(-x_1,-x_2)$. However, because of the electron-electron interaction the system is certainly not invariant under a 90° rotation, and we expect $\Psi(x_2,x_1)\neq\pm\Psi(x_2,x_1)$.

A. Results from exact techniques

The restriction to one spatial dimension allows a number of features of our two-electron system to be calculated without approximation regarding electron correlation, by direct numerical integration of Schrödinger's equation for the Hamiltonian (1) on a large spatial grid. In this way both static and time-dependent, as well as bare-atom and field-dependent, wave functions can be obtained accurately.

First we present a small summary of results for our one-dimensional He analog. They have been obtained by numerical methods described in detail in Ref. [7] for the corresponding H^- analog. For numerical study the He system is placed in a two-dimensional box, one dimension for each electron, which is very large on an atomic scale (axis lengths up to 800 a.u.). The x_1 and x_2 axes are discretized (typically into 1024 mesh points each), and the energies and wave functions for the lowest states are calculated. For example, the ground-state energy is $-2.238\,26$ a.u., the first excited-state energy is -1.704 a.u., and the second excited-state energy is -1.626 a.u. A logarithmic contour plot of the He ground-state probability distribution is shown in Fig. 2 below the corresponding plot for the H^- ground state previously reported [7]. For H^- the ground state is much less localized and has a more pronounced extension along the axes. These axis extensions are confirmations of the familiar mental picture of a negative ion having one of its electrons much closer to the nucleus than the other electron. The lack of invariance under a 90° rotation is evident in

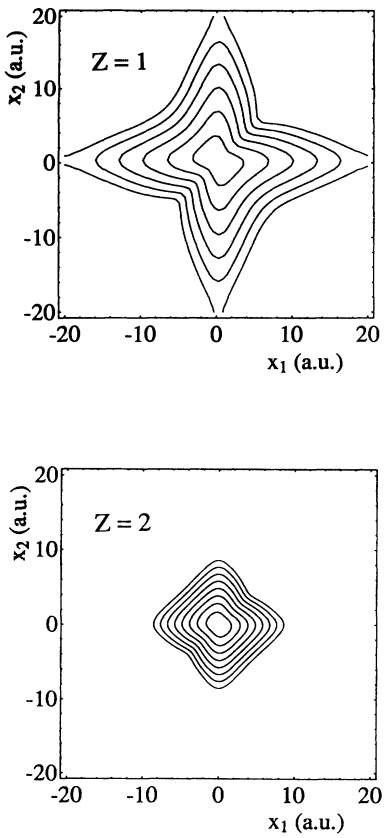

FIG. 2. Logarithmic contour plot of the ground state for $Z=1$ and $Z=2$. Contour lines are drawn at $|\Psi(x_1,x_2)|^2 = 10^{-8}, 10^{-7}$, etc., for both Z.

both cases [9].

We have also calculated the degree of correlation K for the two ground states. This numerical quantity can be uniquely determined for any wave function from the number of relevant coefficients in its canonical representation [10]. The single number $K \geq 1$ represents an effective measure of how many different single-electron orbitals are mixed (i.e., correlated) in a given multiparticle quantum state. It is 1 for a simple product state but can be an order of magnitude larger in some laser-assisted interactions. We have determined K for the 1D He ground state and found $K=1.018$, which is notably smaller than for the ground states of 1D H^-, which has $K=1.094$, although both are still close to 1. Because of the smallness of these K values we can expect a Hartree-Fock type analysis (which assumes a product state and thus $K=1$) to provide fairly accurate approximations to the wave functions and energies. We have similarly examined K for $Z=3-5$, and have found K to decrease monotonically toward 1 as Z increases, indicating that the electron-nucleus interactions dominate over the electron-electron interaction.

We have numerically calculated the first and second ionization thresholds for our helium analog. They are -1.483 a.u. and -0.772 a.u., respectively. These thresholds correspond to the bound-state energies of the (single-electron) Hamiltonian for He^+, whose bound eigenenergies can be immediately obtained by a straightforward numerical diagonalization.

It is important to recognize that there are atomic states with great conceptual usefulness that are to a degree artificial and not directly properties of the atomic Hamiltonian. The most prominent example is an autoionizing state, which is only a convenient discrete labeling for a property that belongs to a range of continuum states. We will be interested in calculating various parameters related to decay and excitation processes for discretely labeled autoionizing states, and so must have a method for constructing these states. We shall apply standard Hartree-Fock (HF) and extended HF techniques for these purposes. At the same time we shall have an unusual opportunity to check HF energies and HF wave functions for lower-energy states against the actual values summarized above.

B. Hartree-Fock analysis

Because the excited states of this two-electron system have not been studied previously, and comparisons with experimental work or the results of other approximate theories are not possible, we will now present a description of our approach to Hartree-Fock calculations in greater detail than would normally be useful [11].

For a state featuring equivalent electrons we seek a real state vector of the product form $|\psi\rangle = |j\rangle \otimes |j\rangle$, where $|j\rangle$ is to be determined. For such a state the expectation value of the energy is

$$\langle jj|H|jj\rangle = 2\langle j|H(\mathrm{He}^+)|j\rangle + \int_{-\infty}^{+\infty} dx\, v_j(x)\psi_j(x)^2 , \tag{3}$$

where $H(\mathrm{He}^+)$ designates the one-electron Hamiltonian of the singly ionized system (He^+ for $Z=2$)

$$H(\mathrm{He}^+)(x) = \frac{p^2}{2} - \frac{Z}{\sqrt{1+x^2}} , \tag{4}$$

and

$$v_j(x) = \int_{-\infty}^{+\infty} dx' \frac{\psi_j(x')^2}{\sqrt{1+(x-x')^2}} \tag{5}$$

denotes an effective electron-electron interaction for the charge density $\psi_j(x)^2$.

The calculus of variations can be used to find a state $|j\rangle$ such that $\delta\{\langle jj|H|jj\rangle - 2\varepsilon_j\langle j|j\rangle\} = 0$, where δ refers to arbitrary, small variations in the wave function $\psi_j(x)$, and where ε_j is a Lagrange multiplier that insures that normalization is unaffected by the variations. Taking $\delta\{\ \} = [\partial/\partial\psi_j\{\ \}]\delta\psi_j$ term by term we obtain

$$\delta[\langle jj|H|jj\rangle - 2\varepsilon_j\langle j|j\rangle] = \int_{-\infty}^{+\infty} \left[-\frac{1}{2}\frac{d^2\psi_j}{dx^2} + \left[\frac{-Z}{\sqrt{1+x^2}} + v_j(x) - \varepsilon_j \right] \psi_j(x) \right] \delta\psi_j(x)\,dx = 0 . \tag{6}$$

Since the variations $\delta\psi_j(x)$ are arbitrary, $\psi_j(x)$ must satisfy an effective, time-independent Schrödinger equation (the Hartree equation)

$$\left[-\frac{1}{2}\frac{d^2\psi_j}{dx^2}+V_{\text{eff}}^{(j)}(x)\right]\psi_j(x)=\varepsilon_j\psi_j(x)\ , \tag{7}$$

where

$$V_{\text{eff}}^{(j)}(x)=\frac{-Z}{\sqrt{1+x^2}}+\nu_j(x)\ . \tag{8}$$

This nonlinear equation can be solved numerically for $\nu_j(x)$ and $\psi_j(x)$ using an iterative procedure in which the output wave function of one iteration is used to calculate the effective potential for the next iteration. There are numerous possible solutions, corresponding to all the $|jj\rangle$ states. Which of these states is obtained depends on the initial seed state chosen for the iteration procedure. The Lagrange multiplier ε_j plays the role of an eigenvalue in the equation if we ignore the fact that the effective potential is dependent upon the "eigenvector" ψ_j. It follows from Eq. (3) that ε_j is related to the total energy of the product state $|jj\rangle$ by

$$\varepsilon_j=\langle jj|H|jj\rangle-\langle j|H(\text{He}^+)|j\rangle\ , \tag{9}$$

i.e., the difference in energy between the two-electron state $|jj\rangle$ of He and the one-electron state $|j\rangle$ of He^+. It follows that $|\varepsilon_j|$ is the binding energy of state $|jj\rangle$—the energy required to remove one electron while leaving the other electron in state $\psi_j(x)$.

For $Z=2$, the HF method provides an approximate ground-state wave function of energy -2.2242 a.u., which is 99.37% of the actual value. It gives the binding energy $|\varepsilon_1|=-0.7502$ a.u., which is 99.39% of the actual value -0.7548 a.u. Although the calculated Hartree-Fock energy of the wave function is very accurate, electron correlation effects are not well taken into account in the wave function. This is made clear by noting that a product-state wave function of the form $\psi_{11}(x_1,x_2)=\psi_1(x_1)\psi_1(x_2)$, which satisfies the necessary symmetry relation $\psi_1(-x)=\psi_1(x)$, also satisfies $\psi_{11}(x_1,x_2)=\psi_{11}(x_2,-x_1)$, so that the wave function is invariant under a 90° rotation. For such a wave function the electrons are just as likely to be on the same side of the nucleus as on opposite sides. The ground-state energies for other Z values are presented in Ref. [7]. Naturally the HF method becomes more accurate with increasing Z, as the electron-nucleus interactions dominate the electron-electron interaction.

We have tested the quality of our state vectors by calculating the rms energy deviation

$$\sigma\equiv[\langle\Psi|H^2|\Psi\rangle-\langle\Psi|H|\Psi\rangle^2]^{1/2}\ , \tag{10}$$

which would be zero for a true eigenstate. For the Hartree-Fock ground state $|1,1\rangle$, the calculated deviation is 0.160 a.u., or about 7% of the total binding energy. Applying the method to state $|2,2\rangle$ gives a solution of energy -1.032 a.u., which lies well above the actual value of the first ionization threshold of -1.483 a.u., suggesting that the system supports an autoionizing resonance near this energy. The deviation of the $|2,2\rangle$ state is 0.261 a.u., indicating that the $|2,2\rangle$ state is not as close an approximation to a true eigenstate as is the $|1,1\rangle$ state.

To find the wave functions for states featuring inequivalent electrons, we take the same Hamiltonian as for the equivalent-electron case, but now we look for states of the form

$$|\psi_{jk}\rangle=\frac{1}{\sqrt{2}}[|jk\rangle+|kj\rangle]\ , \tag{11}$$

which satisfy

$$\delta[\langle\psi_{jk}|H|\psi_{jk}\rangle-\varepsilon_j\langle j|j\rangle-\varepsilon_k\langle k|k\rangle-\varepsilon_{jk}\langle j|k\rangle]=0 \tag{12}$$

for arbitrary, small, independent variations in $\psi_j(x)$ and $\psi_k(x)$. Here ε_j and ε_k are Lagrange multipliers introduced to preserve normalization, and ε_{jk} is a Lagrange multiplier introduced to preserve orthogonality. Equation (12) leads to the coupled equations (the Hartree-Fock equations)

$$\begin{aligned}-\frac{1}{2}\frac{d^2\psi_j}{dx^2}+\left[\frac{-Z}{\sqrt{1+x^2}}+\nu_{kk}(x)-\varepsilon_j\right]\psi_j(x)&=[\tfrac{1}{2}\varepsilon_{jk}-\nu_{jk}]\psi_k(x)\ ,\\ -\frac{1}{2}\frac{d^2\psi_k}{dx^2}+\left[\frac{-Z}{\sqrt{1+x^2}}+\nu_{jj}(x)-\varepsilon_k\right]\psi_k(x)&=[\tfrac{1}{2}\varepsilon_{jk}-\nu_{jk}]\psi_j(x)\ ,\end{aligned} \tag{13}$$

where the electron-electron interaction ν has been generalized to a matrix

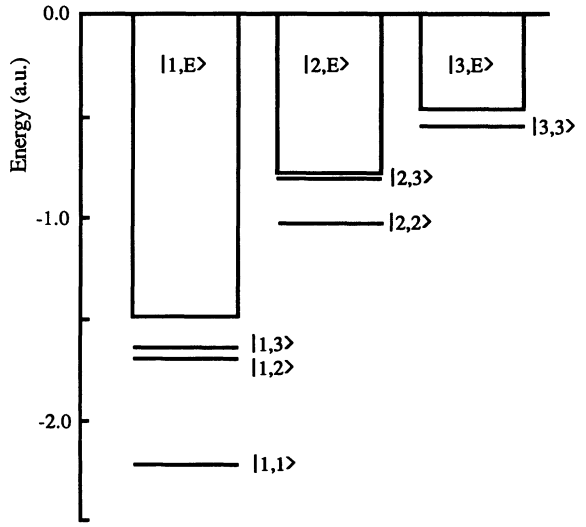

FIG. 3. Energy-level diagram of Hartree-Fock states $|\psi_{ij}\rangle$ for $i,j\leq 3$ and of the $|1,E\rangle$, $|2,E\rangle$, and $|3,E\rangle$ continua. The threshold energies were obtained through a direct diagonalization of the one-electron Hamiltonian for He^+.

TABLE I. Energies, binding energies (E_{BE}), predicted thresholds, and rms-energy deviations of Hartree-Fock states for $Z=2$.

State	$\langle H \rangle$ (a.u.)	Binding energies (a.u.)	$\langle H \rangle + E_{BE}$ (a.u.) $n=1$	$n=2$	$n=3$	Deviation (a.u.)
$\|1,1\rangle$	−2.224	0.750	−1.474			0.160
$\|1,2\rangle$	−1.702	0.223	−1.479			0.065
		1.058		−0.644		
$\|1,3\rangle$	−1.636	0.161	−1.475			0.195
		1.227			−0.408	
$\|2,2\rangle$	−1.032	0.272		−0.760		0.256
$\|2,3\rangle$	−0.808	0.039		−0.769		0.085
		0.580			−0.228	
$\|3,3\rangle$	−0.546	0.101			−0.454	0.261
Actual continuum thresholds (a.u.):			−1.483	−0.772	−0.465	

$$v_{mn}(x)=\int_{-\infty}^{+\infty} dx' \frac{\psi_m(x')\psi_n(x')}{\sqrt{1+(x-x')^2}} . \tag{14}$$

If the diagonal elements $v_{jj}(x)$ and $v_{kk}(x)$ represent the averaged electrostatic electron-electron interaction, then the off-diagonal elements constitute an effective "exchange potential." The Lagrange multipliers ε_j and ε_k can be interpreted as (minus) the binding energies of the electrons.

The coupled equations (13) can also be solved by an iterative numerical procedure. Which solution is obtained depends again critically on the initially chosen seed vector. Examples of states we have found for helium include the singly excited states $|\psi_{12}\rangle$ and $|\psi_{13}\rangle$ and the doubly excited state $|\psi_{23}\rangle$. In Fig. 3 we present a diagram showing the energies of all Hartree-Fock states $|\psi_{ij}\rangle$ for $i,j \leq 3$ and of the three lowest threshold continua of He^+. Table I summarizes the result for the discrete states. Included in the table are the sums of the total energies and the binding energies. These sums correspond to the energy which the residual electron would have if the other electron were suddenly to disappear. Because no adjustment in the residual electron's wave function is made, the residual wave function is not an eigenvector of one-dimensional He^+. For example, if the lower-energy electron of the $|1,3\rangle$ state were to disappear, the remaining electron would have energy −0.408 a.u., whereas an electron in the $n=3$ state of He^+ would have energy −0.465. This illustrates clearly that the excited-state component of $|1,3\rangle$ is a higher energy state than the $n=3$ excited state of He^+.

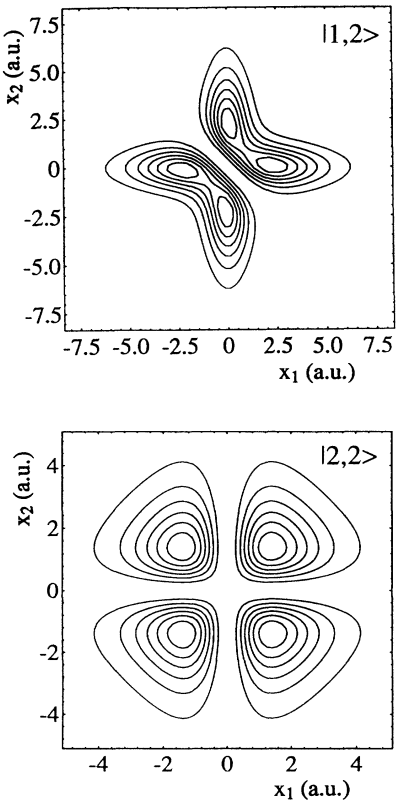

FIG. 4. Linear contour plots of the Hartree-Fock $|1,2\rangle$ and $|2,2\rangle$ states. The spatial scales and contour heights differ in the two plots.

The small rms energy deviation shown in Table I for states $|1,2\rangle$ and $|2,3\rangle$ is noteworthy. In these states, one electron is in an even-parity state and one in an odd-parity state. Such combinations need not be invariant under a 90° rotation. For example

$$\begin{aligned}\psi_{jk}(x,-x)&=(1/\sqrt{2})[\psi_j(x)\psi_k(-x)+\psi_k(x)\psi_j(-x)]\\&=(1/\sqrt{2})[\psi_j(x)\psi_k(x)-\psi_k(x)\psi_j(x)]\\&=0\neq\psi_{jk}(x,x) .\end{aligned}$$

It follows that electron-electron correlation effects can be taken more fully into account for these states than for even-even or odd-odd combinations. This alternative symmetry is clearly seen in the contour plots of the spatial wave functions of the Hartree-Fock $|1,2\rangle$ and $|2,2\rangle$ states (Fig. 4).

C. Basis-state diagonalization

The Hartree-Fock method can be extended in various ways to account more fully for the electron-electron interaction and for correlation, which is manifested

mathematically as a coupling between the solutions of the Hartree-Fock equations. Because the "effective potentials" in the HF equations vary from state to state, some effort is required to find each solution, and the solutions obtained for different states need not be orthogonal to each other. To avoid the difficulties associated with these nonorthogonalities, one can select a single, complete orthonormal basis set with which to work. We have worked with two such basis sets. For the first set, which we shall refer to as the HF basis set, we began by solving Eq. (8) for the HF ground state $|1\rangle$ and for the corresponding effective potential $V_{\rm eff}^{(1)}(x)$ defined in (8). We then defined a single-electron Hamiltonian using this particular effective potential,

$$H^0=\frac{p^2}{2}+V_{\rm eff}^{(1)} , \tag{15}$$

and we numerically solved the eigenvalue equation $H^0|j\}=\varepsilon_j|j\}$ for the full set of eigenvalues and eigenvectors. We thus obtained the two-electron basis set $\tilde{\psi}_{jk}(x_1,x_2)=\langle x_1x_2|jk\}$, where

$$|jk\}=\begin{cases}|j\}|j\}\ , & j=k\\ \frac{1}{\sqrt{2}}(|j\}|k\}+|k\}|j\})\ , & j\neq k\ .\end{cases} \tag{16}$$

The state $|11\}$ thus corresponds to the HF ground state, but the other states are not solutions of the Hartree-Fock equations. Since $V_{\rm eff}^{(1)}(x)$ has even parity, the basis states satisfy $\tilde{\psi}_{jk}(-x_1,-x_2)=(-1)^{j+k}\tilde{\psi}_{jk}(x_1,x_2)$. The full Hamiltonian H is related to H^0 by

$$H(x_1,x_2)=H^0(x_1)+H^0(x_2)+W(x_1,x_2) , \tag{17}$$

where

$$\begin{aligned}W(x_1,x_2)&=V(x_1,x_2)-V_{\rm eff}^{(1)}(x_1)-V_{\rm eff}^{(1)}(x_2) ,\\ &=\frac{1}{\sqrt{1+(x_1-x_2)^2}}-v_{11}(x_1)-v_{11}(x_2) .\end{aligned} \tag{18}$$

The residual electron-electron interaction W couples the basis states. However, because $W(-x_1,-x_2)=W(x_1,x_2)$, the interaction does not mix states of opposite symmetry.

For a chosen N-point x-axis grid, there are N states $|j\}$ and $(N^2+N)/2$ unique basis states. In order to find the exact eigenvectors it would be necessary to find the matrix elements of W between all such states and to diagonalize the full Hamiltonian matrix H. We have limited our number of basis states to approximately 775 states of each symmetry and have diagonalized the Hamiltonian in the resulting limited Hilbert space. The calculation time is greatly reduced by taking advantage of hermiticity and by noting that in the spatial integrations we usually need not go far from either axis. We have found that this size basis set is suitable for our present purposes.

The lowest-energy eigenvector $|\alpha\rangle$ of the Hamiltonian in the limited Hilbert space spanned by the truncated HF basis has eigenvalue -2.2355 a.u., which is 99.88% of the actual value. The rms-energy deviation σ of the state [recall Eq. (10)] is 0.094 a.u., or 4.2% of the binding energy. All the eigenvectors of course are obtained as linear combinations of the basis states $|jk\}$. For the ground state $|g\rangle$ we find that the seven largest expansion coefficients are $\{1,1|g\rangle=0.9959$, $\{2,2|g\rangle=0.0623$, $\{2,4|g\rangle=0.0281$, $\{2,6|g\rangle=0.0152$, $\{2,8|g\rangle=-0.010$, $\{1,3|g\rangle=-0.009$, and $\{3,3|g\rangle=0.008$. The importance of the doubly excited basis states in the ground state can easily be understood. Since W does not mix states of opposite symmetry, the expansion coefficient $\{jk|g\rangle$ is nonzero only if $j+k$ is even; $|j\}$ and $|k\}$ can both be even-parity states (in which case the indices j and k are both odd), or $|j\}$ and $|k\}$ can both be odd-parity states (in which case the indices are both even). If $|j\}$ and $|k\}$ are both even-parity states—as is the case for the entire manifold $|1k\}$ of singly excited or singly ionized states—then $\tilde{\psi}_{jk}(x,-x)=\tilde{\psi}_{jk}(x,x)$. On the other hand, if $|j\}$ and $|k\}$ both have odd parity, then $\tilde{\psi}_{jk}(x,-x)=-\tilde{\psi}_{jk}(x,x)$. It is only by taking a linear combination which includes both even-even and odd-odd basis states that we can have $|\Psi(x,-x)|^2\neq|\Psi(x,x)|^2$. It is the electron correlation effects which produce this inequality and which our Hartree-Fock ground and basis state $|1,1\}$ was missing.

The diagonalization of the odd-parity Hilbert space of basis states gives a first excited state $|\beta\rangle$ of energy -1.704 a.u. and rms-deviation 0.042 a.u., which can be compared with the respective values -1.702 a.u. and 0.065 a.u., which were quoted above for the Hartree-Fock first excited state.

A second basis set which we have used consists of product states of He^+ eigenstates. Thus, the H^0 of Eq. (15) is replaced by $p^2/2-2/(1+x^2)^{1/2}$, and $W(x_1,x_2)$ becomes simply $1/[1+(x_1-x_2)^2]^{1/2}$. We have found that using the same size basis set as before gives slightly better results than the previous ones. We obtain a ground state of energy $-2.238\,01$ a.u., which is 99.99% of the actual value, and rms-deviation 0.047 a.u., or 2.1% of the energy. The first excited state has energy -1.705 a.u. and deviation 0.018 a.u.

III. AUTOIONIZING STATES

A. Static structure

The diagonalization procedure described in Sec. II C provides a sequence of singly excited bound states leading into the single-ionization continuum, and eventually into the double-ionization continuum. We shall denote the continuum eigenstates by $|\varepsilon\rangle$, where ε is the total, two-electron energy. Doubly excited "bound" states were part of the basis set, but the diagonalization process has enfolded them into the continuum so that they do not appear explicitly in the sequence, and are manifested only as continuum resonances. Figure 5 shows the square of the continuum wave functions $\langle x_1x_2|\varepsilon\rangle$ for three energies: $\varepsilon=-1.30$ a.u., $\varepsilon=-1.05$, a.u. near the energy -1.03 a.u. of the Hartree-Fock $|2,2\rangle$ state, and $\varepsilon=-0.90$ a.u. (The states were calculated using the HF basis.) If there were no resonance, one would expect the wave function to exhibit no sharp features near the origin. Such featureless wave functions were obtained, for example, in an earlier study [7] of the corresponding $Z=1$ atom (negative ion). Some structure near the origin

is present in all three plots, indicating a very broad energy range for the resonance. The wave functions are real and standing-wave superpositions of incoming and outgoing scattering states.

In order to define discrete autoionizing states and to describe the resonance in the manner introduced by Fano [8], the autoionizing states must be distinguished from the continuum. They should be orthogonal to each other and to the continuum in which they are embedded. Ideally, the only coupling would be between each autoionizing state and the continuum, without any coupling between the autoionizing states or between continuum states of different energy. Then each autoionizing state could be said to decay independently into the continuum. We can achieve such a situation by partitioning our Hilbert space of basis states into two orthogonal subspaces, one part which we shall call P consisting of the continuum $|1,E\}$ (i.e., our basis-state approximation to those states in which one electron is in the ground state and the other is not bound), and the second part Q consisting of all remaining states, namely, the basis-state approximations to the ground state, to singly excited but unionized states, and to all doubly excited and doubly ionized states. The P subspace can then be diagonalized to obtain a single-electron continuum $\{|\varepsilon\rangle_P\}$, and the Q subspace can be diagonalized to obtain a set of states $|\alpha\rangle_Q$, $|\beta\rangle_Q, \ldots$, consisting of close approximations to the ground state and the singly excited states, and also containing the autoionizing states, the remaining single-electron continua, and the doubly ionized continuum. Each state in one subspace is then coupled by W [recall (18)] to each state of the same parity in the other subspace. Because this partitioning of the Hilbert space is directly dependent upon which basis set has been chosen, the states one obtains from a diagonalization of the Hamiltonian within the individual subspaces will also depend upon the basis set. We shall return to this point later. For now we proceed using the Hartree-Fock basis described in the previous section.

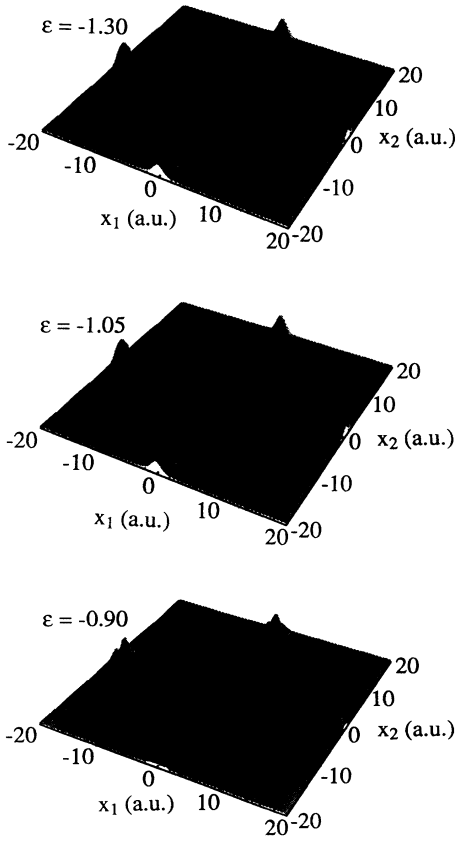

FIG. 5. Square of the continuum wave functions, $\langle x_1 x_2|\varepsilon\rangle^2$, for energies $\varepsilon=-1.30$, -1.05, and -0.90. The three plots have the same vertical scale.

Through the above procedure we can easily identify the lowest-energy doubly excited state, which we shall call $|a\rangle$. Other autoionizing states are also present, but are of much less importance, and we shall focus our discussion on $|a\rangle$. A random-dot stereogram of the spatial wave function is shown in Fig. 6. Three-dimensional and contour plots of the square of the wave function are also shown in the first row of Fig. 7. This state has energy $E_a=\langle H\rangle=-1.054$ a.u. and rms-energy-deviation 0.162 a.u., which is 38% less than the deviation of the $|2,2\rangle$ state that was obtained by solving the Hartree equation. The latter state was invariant (to within a sign) under a 90° rotation. The new state $|a\rangle$ clearly lacks the invariance, while still preserving the necessary symmetry about the lines $x_2=x_1$ and $x_2=-x_1$. Thus effects of the electron-electron interaction are clearly present in state $|a\rangle$, although of course incompletely since the state would be unstable if they were fully taken into account. The remaining correlation effects result in a coupling W between $|a\rangle$ and the singly excited continuum $\{|\varepsilon\rangle_P\}$. It is this coupling which allows the state $|a\rangle$ to autoionize, as discussed in Sec. III B and shown in the remaining rows of Fig. 7.

B. Time dependence of the autoionizing state

To further understand the lowest-energy autoionizing state, we investigate the dynamical behavior of the system for the initial condition $\Psi(x_1,x_2;0)=\langle x_1,x_2|a\rangle$, i.e., we study the dynamics of the autoionization of state $|a\rangle$ by numerically solving the Schrödinger equation

$$i\frac{\partial\Psi(x_1,x_2;t)}{\partial t}=\left[\frac{p_1^2}{2}+\frac{p_2^2}{2}+V(x_1,x_2)\right]\Psi(x_1,x_2;t) \tag{19}$$

on the two-dimensional, 1024×1024 spatial lattice described above. In principle we could determine the time dependence of the wave function from its expansion in the energy eigenbasis. However, this would not be practical due to the very large storage requirements or computational time that would be required. Each of the 775 basis states would either need to be stored as a 1024×1024 dimensional matrix, or frequently recalculated as the appropriate linear combination of product states. Further, it is not clear that our 775 basis states would be sufficient to give accurate results—the full system contains over 5×10^5 basis states.

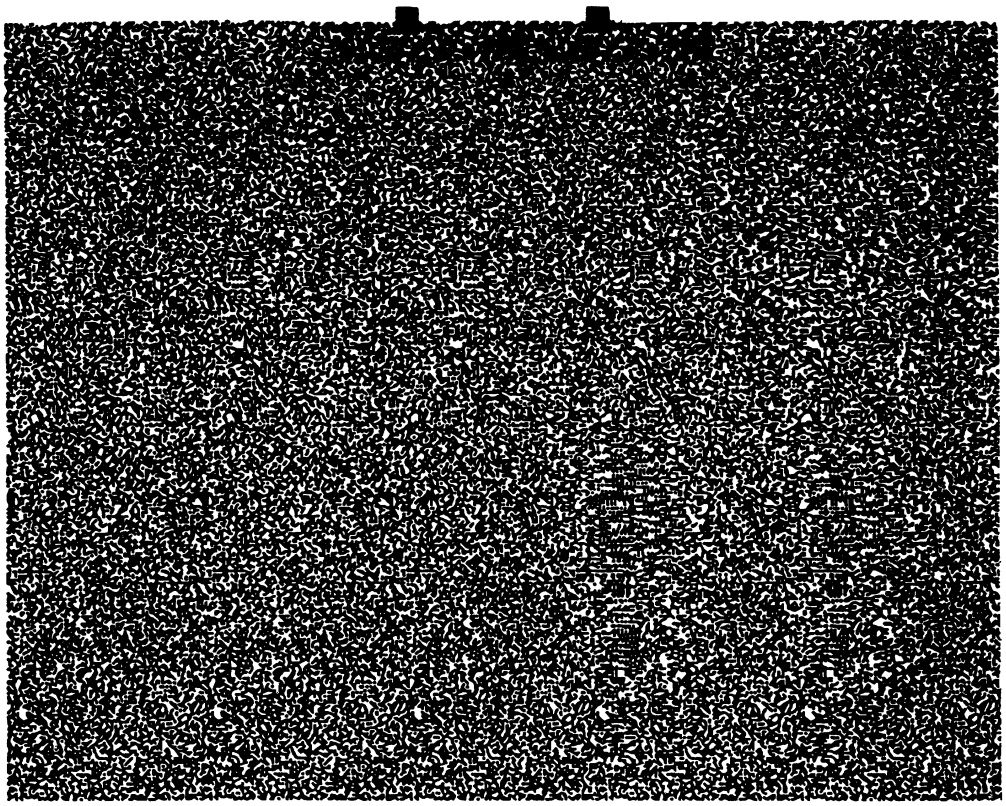

FIG. 6. Three-dimensional image of the spatial wave function of $|a\rangle$ vs x_1 and x_2, seen directly from above. To see the image, one should focus one's eyes *behind* the plane of the page in such a way that the two large black spots near the top center of the field are seen as three (not two or four) spots. This can often be done by first holding the page near one's face with the eyes relaxed and then slowly moving the page outward while watching the large spots [12]. A plot of the square of the wave function is shown in the top row of Fig. 7.

To circumvent these computational difficulties we have performed a direct calculation of $\Psi(x_1,x_2;t)$ by solving the time-dependent Schrödinger equation on a 1024×1024 spatial grid. For each individual time step the time-evolution operator is split into the actions of the kinetic-energy operator and the spatial potential

$$\exp(-iH\Delta t)=\exp[-i(p_1^2+p_2^2)\Delta t/4]\times\exp[-iV(x_1,x_2)\Delta t]\times\exp[-i(p_1^2+p_2^2)\Delta t/4]+O(\Delta t^3)\ . \quad (20)$$

Fast-Fourier transforms of the wave function are performed as needed so that action of the kinetic-energy operators is determined in momentum space. Details about the numerical techniques can be found in Ref. [7].

We use $\Psi(x_1,x_2;t)$ to examine the time dependence of various spatial probabilities and various bound-state probabilities for the decay rate from the initial state. Some of our results are shown in Figs. 7 and 8. The left-hand column displays the spatial probability density $|\Psi(x_1,x_2;t)|^2$ vs x_1 and x_2 at various times, and the right-hand column displays contour plots of the same quantity.

The first row in Fig. 7 shows the probability density for the initial state, as discussed in Sec. II A. By $t=2$ a.u., shown in the second row, each of the two peaks which were along the e-e repulsion line $x_2=x_1$ has split into a doublet, and population has traveled to the energetically favored diagonal $x_2=-x_1$. By $t=4$ a.u., a small peak has formed at the origin, and peak heights begin to diminish as the population becomes less localized in space. Figure 8 continues the sequence. The seven-peak structure is maintained at longer times as the population begins to move outward along the axes. A small amount of "sloshing" is also visible in the outgoing population.

One can define an effective single-electron density from the two-electron wave function by integrating over either of the two spatial variables, say x_2,

$$\rho(x;t)\equiv\int_{-\infty}^{\infty}dx_2|\Psi(x,x_2;t)|^2\ . \quad (21)$$

Figure 9 shows the time development of this density on the time scale of Figs. 7 and 8. The figure shows clearly the change from the initial two-peak structure characteristic of a first excited state to a single-peak structure characteristic of the ground state of the remaining He^+.

The sequence begun in Figs. 7 and 8 is continued in Fig. 10, which shows the spatial probability density for the longer times $t=20$ a.u. and $t=50$ a.u. on a larger scale than was used for the shorter times. The $t=20$ a.u.

plot shows the first "pulse" of population going out along the axes. The concentration of the probability along the axes clearly indicates that only one electron can escape from the nucleus. Figure 11 shows $\rho(x;t)$ for times $t=50$ and 150 a.u. and clearly shows the spatial form of the population distribution for the outgoing, autoionized electron. These packets move with a kinetic energy which corresponds to the energy of state $|a\rangle$ above the first threshold. The narrow peak at $x=0$ which goes beyond the vertical scale of the graph corresponds to the He^+ ground state. After 150 a.u. the area under the curve between ± 10 a.u. is only 0.01 greater than its asymptotic value of 0.50.

In Fig. 12(a) we show the time development of the population of the decaying state,

$$P(t)\equiv|\langle\Psi(0)|\Psi(t)\rangle|^2=|\langle a|\Psi(t)\rangle|^2 . \tag{22}$$

The best exponential fit $[\exp(-\gamma_d t)]$ to the data is shown as the dashed curve. We find $\gamma_d=0.050$ a.u. We also note that the decay curve exhibits oscillations. These oscillations can be understood by analyzing the decay process using the alternative basis site of product states of the one-electron He^+ Hamiltonian. This alternative set, which totally ignores the electron-electron interaction, describes well the final, asymptotic state of the autoionization process as one electron escapes to infinity. We chose in Sec. II to use a particular basis set whose lowest-energy state was the Hartree-Fock ground state. However, the "decay continuum" $\{|\varepsilon\rangle_P\}$, which resulted from that choice of basis, does not correspond directly to the actual asymptotic state of the decay process.

In Fig. 12(b) we display the time-dependent probabilities for finding at least one electron in the three lowest-lying bound states of the core system He^+ during the decay of state $|a\rangle$. These probabilities can be easily obtained by appropriate projections [7]. The probability of finding at least one electron in the He^+ ground level, denoted by P_1, is vanishingly small for the $t=0$ autoionizing state. Clearly as the autoionizing state decays, one electron drops into the He^+ ground level, and $P_1(t)$ increases with t to its final value of 1. The quantities P_1, P_2, and P_3 correspond respectively to the total populations of the $|+1,n\}$, $|+2,n\}$, and $|+3,n\}$ $(n=1,2,\ldots)$ manifolds of $He^+\otimes He^+$ product states, where we have included a + sign in the ket to designate states of the He^+ basis. (Some overcounting occurs since states such as $|+1,3\}$ are in both the P_1 and P_3 manifolds.) Our initial state $|a\rangle$ is mainly a linear combination of states in

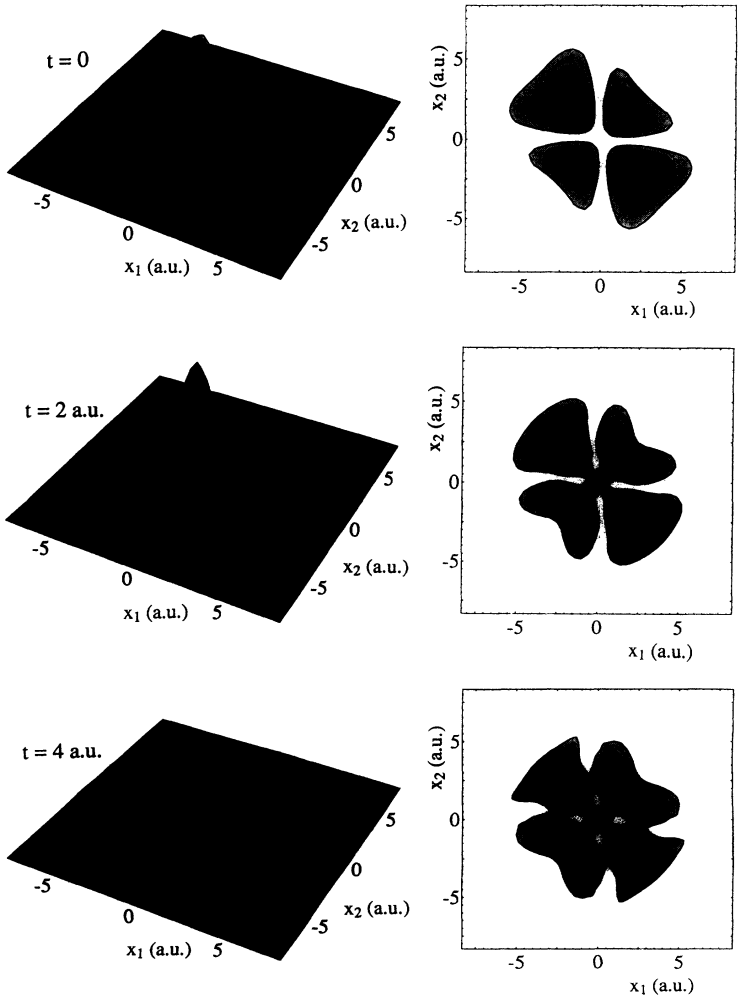

FIG. 7. Three-dimensional and contour plots of the two-electron probability $|\Psi(x_1,x_2;t)|^2$ as a function of the electron coordinates x_1 and x_2 at time $t=0$, 2, and 4 a.u. The vertical scaling and contour levels are consistent for the different times.

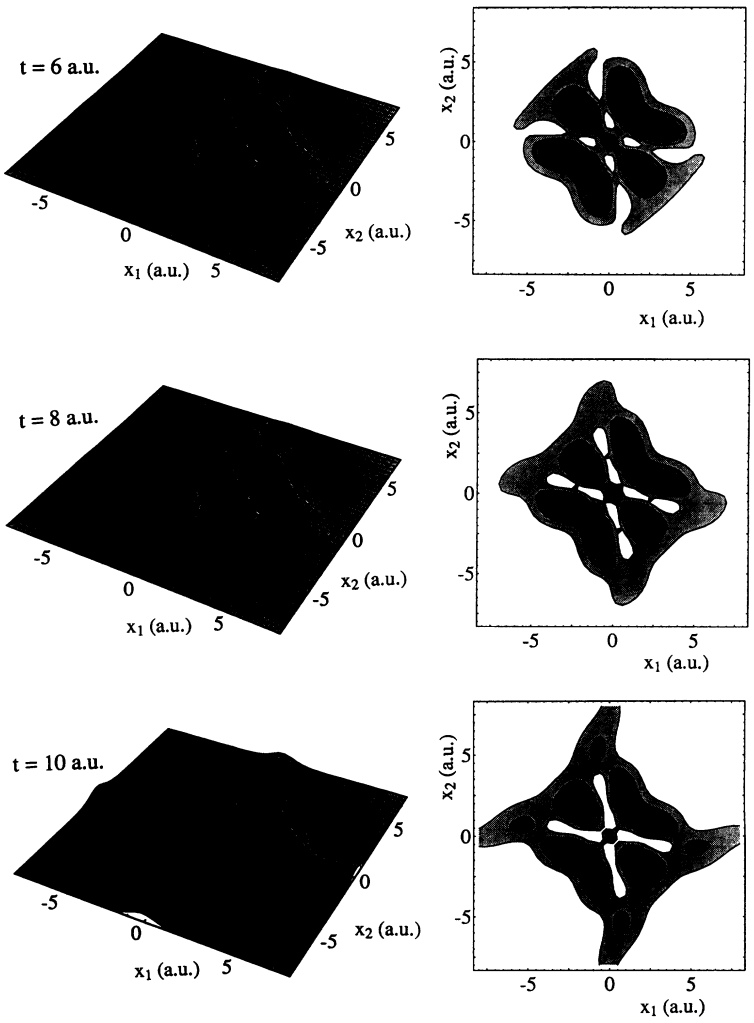

FIG. 8. Similar to Fig. 7, but at times $t=6$, 8, and 10 a.u. Scales are the same as in Fig. 7.

the P_2 and P_3 manifolds, with 93% of the population lying in the P_2 manifold and 7% in the P_3 manifold. The state $|+2,3\}$, which lies in both manifolds, has the incorrect symmetry to be populated. Important individual states are $|+2,2\}$ with 81% of the population and $|+3,3\}$ with 7%, or nearly all the population of the P_3 manifold. The decay process defies simple description because of the very large number of states and couplings (discrete state–discrete state, discrete state–continuum, and continuum–continuum) which are present. We note, however, that the difference in energy-expectation values $\{+3,3|H|+3,3\}-\{+2,2|H|+2,2\}=0.492$ a.u. and the matrix element $\{+2,2|H|+3,3\}=0.114$ a.u. combine to give an effective "Rabi frequency" $[0.492^2+4(0.114^2)]^{1/2}$ a.u.$=0.542$ a.u., which is within 3% of the frequency 0.561 a.u. which we obtain from the oscillations in Fig. 12(b) by noting that the period of the oscillation is 11.2 a.u.

These oscillations would be greatly diminished if we had worked from the beginning with the He^+ basis states. The decay continuum would then correspond to the actual asymptotic continuum. Our patitioning of the full Hilbert space would result in a slightly different subspace for defining the autoionizing state, which we denote by $|+a\rangle$. In this case the couplings between all the discrete states of the $|+2,n\}$ and $|+3,n\}$ manifolds would be acounted for in defining the new autoionizing state $|+a\rangle$. This autoionizing state can be thought of as a single "dressed state" which decays into the $|+1E\rangle$ continuum [13]. The state has energy $\langle+a|H|+a\rangle=-1.045$ a.u. and rms-energy-deviation 0.12 a.u. In order to check our conjecture we show the decay of the autoionizing state $|+a\rangle$ in Fig. 12(c). Indeed, the oscillations have basically disappeared. The smoothness of the temporal decay curve of $|+a\rangle$ suggests that the He^+ basis set is superior to the Hartree-Fock basis set for this case and that $|+a\rangle$ can be considered to be an alternative representation of the lowest-energy autoionizing state.

In Fig. 13 we display the kinetic-energy distribution $P(E)$ of the electrons at time 150 a.u. after $|a\rangle$ begins its decay. This distribution was obtained from the corresponding two-electron wave function in momentum space, an integration of one momentum and a rescaling to energy. The main peak arises from the autoionized electron and occurs at energy 0.434 a.u., which is consistent

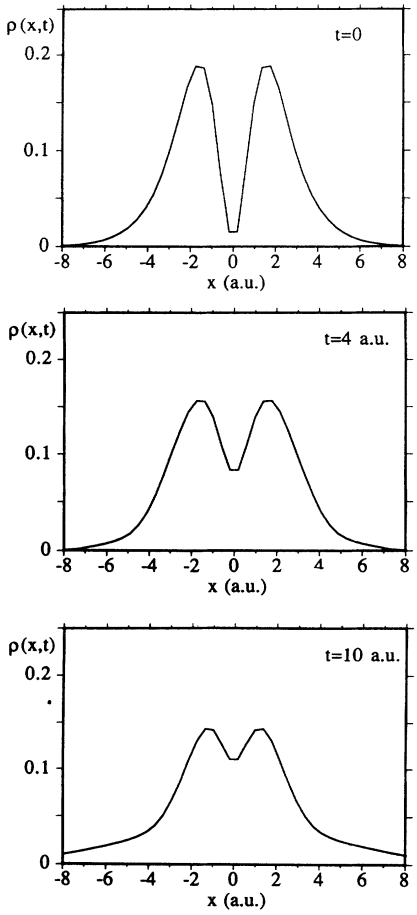

FIG. 9. Single-electron densities $\rho(x;t)$, as defined in the text [Eq. (21)] for times $t=0$, 4, and 10 a.u.

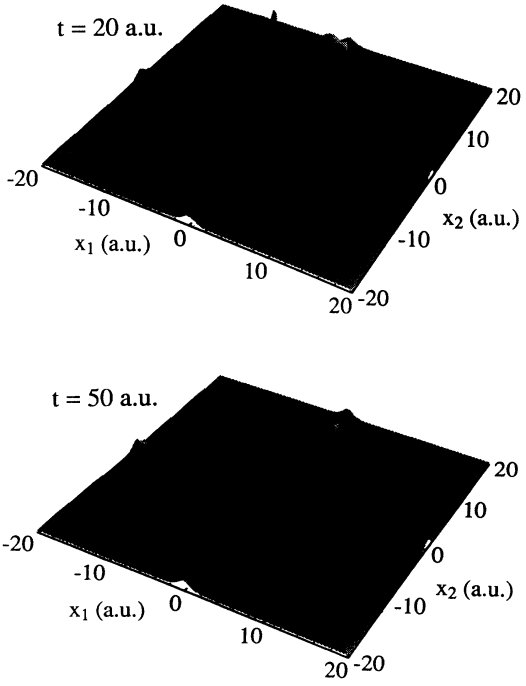

FIG. 10. Three-dimensional plots similar to Fig. 7, but for times $t=20$ and 50 a.u. The vertical scales are consistent for the two times, but both the vertical and spatial scales are changed from Fig. 7.

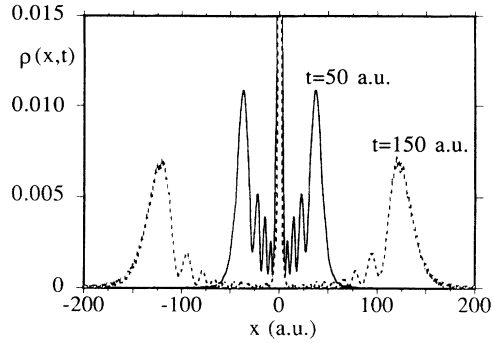

FIG. 11. Single-electron density $\rho(x;t)$ for $t=50$ and 150 a.u. on a larger spatial scale.

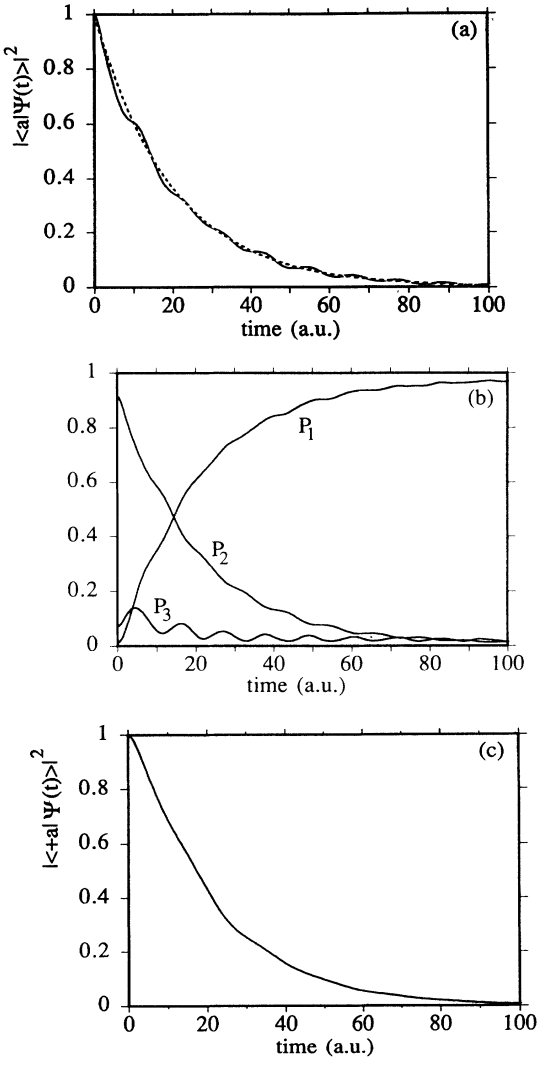

FIG. 12. (a) The time dependence of the overlap $|\langle\Psi(0)|\Psi(t)\rangle|^2$ for an initial state $|\Psi(0)\rangle=|a\rangle$. The dashed line represents the fitted exponential decay with a decay constant $=0.050$ a.u. (b) The time dependence of the probabilities P_i to find at least one electron in the ith bound state of the (one-electron) core system He^+. The core ground state $[P_1(t)]$ gets populated as the autoionizing state decays. Note the oscillatory structure in the probability $P_3(t)$ corresponding to the second excited state in He^+ and the $|+3,n\}$ manifold of He^+ product states. (c) The time dependence of the overlap $|\langle\Psi(0)|\Psi(t)\rangle|^2$ for an initial state $|\Psi(0)\rangle=|+a\rangle$.

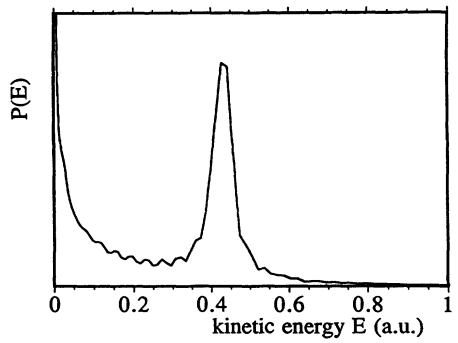

FIG. 13. Kinetic-state distribution of the electrons.

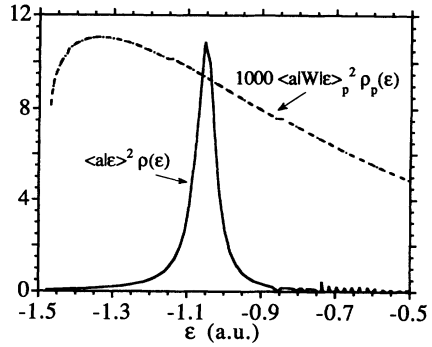

FIG. 14. The solid curve denotes the projection of the autoionizing state onto the fully diagonalized continuum, $\langle a|\varepsilon\rangle^2\rho(\varepsilon)$. The dashed curve gives the coupling $\langle a|W|\varepsilon\rangle_p^2\rho_p(\varepsilon)$ between $|a\rangle$ and the singly excited continuum $|\varepsilon\rangle_p$ vs ε. The solid curve should represent the kinetic energy of the autoionized electron, once the threshold energy is taken into account.

with the energy difference 0.438 a.u. between the autoionizing state (at -1.045 a.u.) and the first ionization threshold (at $\varepsilon=-1.483$ a.u.). The full width at half maximum γ_a as read off the graph is 0.05 a.u. The bound electron contributes to the lower-energy portion of the graph.

The decay of the autoionizing state $|a\rangle$ is caused by the electron-electron interaction W of Eq. (18). In Fig. 14 we plot the square of this coupling between $|a\rangle$ and the continuum $\{|\varepsilon\rangle_p\}$, multiplied by the appropriate density of states factor $\rho_p(\varepsilon)$, as a function of the total (two-electron) energy. We also show the square of the projection of $|a\rangle$ onto the full continuum $|\varepsilon\rangle$, multiplied by the density of states factor $\rho(\varepsilon)$. The Fermi golden rule decay rate of the state is

$$\Gamma=2\pi\rho_p(\varepsilon)\langle a|W|\varepsilon\rangle_p^2=0.059 \text{ a.u.} , \tag{23}$$

which is consistent with the width of the projection $\rho(\varepsilon)\langle a|\varepsilon\rangle^2$ evaluated at $\varepsilon=E_a$. Thus the lifetime of this autoionizing state is approximately $1/\Gamma=17$ a.u. (The decay rate of the alternative autoionizing state $|+a\rangle$ can be calculated by similar methods to be 0.053 a.u., so that its lifetime is 19 a.u.)

IV. DIPOLE MATRIX ELEMENTS

The ground state $|\alpha\rangle$ and the autoionizing state $|a\rangle$ have the same spatial parity and are not dipole coupled. Therefore we turn our attention to the dipole matrix element between the first excited state $|\beta\rangle$ and the full continuum $\{|\varepsilon\rangle\}$. We will estimate the value of the Fano q parameter for the state $|a\rangle$. The solid curve in Fig. 15 shows $\langle\beta|(x_1+x_2)|\varepsilon\rangle^2$, times the appropriate density of continuum states factor $\rho(\varepsilon)$. The graph is dominated by a continuum resonance arising from the lowest-energy autoionizing state. Figure 15 also presents the modulus squared of the dipole coupling between the first excited state $|\beta\rangle$ and the p continuum {denoted by $|\varepsilon\rangle_p$}, times its density of states factor $\rho_p(\varepsilon)$.

The subsystem consisting of the first excited state $|\beta\rangle$, the autoionizing state $|a\rangle$, and the "singly excited" continuum $\{|\varepsilon\rangle_p\}$ satisfy the criteria of the Fano model. The q parameter for the autoionizing resonance is defined as

$$q(\varepsilon)=\frac{\langle\beta|(x_1+x_2)|a\rangle+\mathrm{P}\int_{\varepsilon_{\min}}^{\infty}\frac{\langle\beta|(x_1+x_2)|\varepsilon'\rangle_{pp}\langle\varepsilon'|W|a\rangle}{\varepsilon-\varepsilon'}\rho_p(\varepsilon')d\varepsilon'}{\pi\langle\beta|(x_1+x_2)|\varepsilon\rangle_{pp}\langle\varepsilon|W|a\rangle\rho_p(\varepsilon)} , \tag{24}$$

where P denotes the principal-value integral over all energies in the $\{|\varepsilon\rangle_p\}$ continuum. We calculated $\langle\beta|(x_1+x_2)|a\rangle=-1.17$ a.u. The principal-value integral can be calculated using the data illustrated in Fig. 15. Because we have a discretized continuum, the integral becomes a sum over discrete energies. To maintain symmetry about the singularity at $\varepsilon'=\varepsilon$, we evaluate the sum for ε midway between our continuum energies. Over much of the continuum, the principal-value integral is of order 10^{-3} a.u. (-0.0045 a.u. at $\varepsilon=E_a$), so it is relatively unimportant in evaluating q. For our system Eq. (24) gives $q=-24$, which should be seen as an estimate and not as a precise calculation, because of the truncation of the set of basis states [14].

The standard Fano formalism predicts that matrix elements to the diagonalized and undiagonalized continua are related by

$$\langle\beta|(x_1+x_2)|\varepsilon\rangle^2\rho(\varepsilon)=f(\varepsilon)\langle\beta|(x_1+x_2)|\varepsilon\rangle_p^2\rho_p(\varepsilon) , \tag{25}$$

where $f(\varepsilon)$ is the Fano profile factor,

$$f(\varepsilon)=\frac{(\varepsilon-\tilde{E}_a+q\Gamma/2)^2}{(\varepsilon-\tilde{E}_a)^2+\Gamma^2/4} . \tag{26}$$

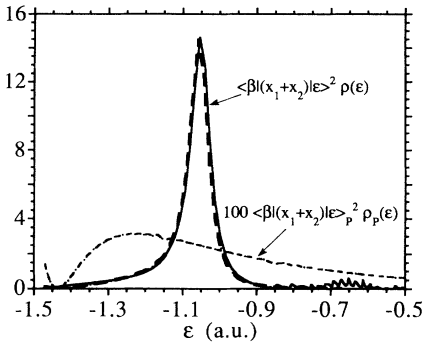

FIG. 15. The solid curve is $\langle\beta|(x_1+x_2)|\varepsilon\rangle^2\rho(\varepsilon)$. The curve with fine dashes denotes $100\langle\beta|(x_1+x_2)|\varepsilon\rangle_p^2\rho_p(\varepsilon)$ and the curve with larger dashes $f(\varepsilon)\langle\beta|(x_1+x_2)|\varepsilon\rangle_p^2\rho_p(\varepsilon)$, where $f(\varepsilon)$ is defined in Eq. (24).

In $f(\varepsilon)$, $\tilde{E}_a$ denotes an effective energy of the autoionizing state which is slightly shifted from E_a through the interaction with the continuum. The shift is given by the principal-value integral $\mathrm{P}\int_{\varepsilon_{\min}}^{\infty}\langle a|W|\varepsilon'\rangle_p^2\rho_p(\varepsilon')/(\varepsilon-\varepsilon')d\varepsilon'$, which for our system evaluates to 0.0015 a.u. in the vicinity of $\varepsilon=E_a$. The product $f(\varepsilon)\langle\beta|(x_1+x_2)|\varepsilon\rangle_p^2\rho_p(\varepsilon)$ is shown as the dashed line in Fig. 15 for $q=-24$ and $\Gamma=0.059$ a.u. The width of the curve matches well with the solid curve. The overall similarity of the dashed and solid curves indicates the applicability of the Fano formalism to the present system and the internal consistency of our results.

Equation (26) predicts a Fano minimum at $\varepsilon=\tilde{E}_a-q\Gamma/2$. For our parameters, this minimum would lie far outside the energy range in which $|a\rangle$ can be regarded as an isolated autoionizing state, and thus no Fano minimum is present in Fig. 15.

V. SUMMARY AND CONCLUSIONS

We have studied the bound and continuum structure of one-dimensional helium using Hartree-Fock, basis-state diagonalization and exact numerical techniques. We have used symmetry considerations to discuss the strengths and weaknesses of the Hartree-Fock approach, and have noted how states of different symmetry must be superposed to take electron-electron correlation effects into account. We have found that the model has many of the features of the true helium atom, including a Rydberg series of singly excited states below the first threshold and a structured continuum which can be described in terms of autoionizing states. Both electrons are tightly bound in the ground state of the model, in contrast to the ground state of the $Z=1$ model of H^-, which featured an "inner" and "outer" electron [7].

We have examined different possible definitions of the lowest-energy autoionizing resonance for our system, which can lead to different temporal features in the decay of the state. Specifically, quantum beats can occur in the decay so that the state does not decay exponentially. We have shown that the quantum beats can be reduced if the autoionizing state is defined as an eigenstate in a subspace of both singly and doubly excited states that is chosen so as to be orthogonal to the final, asymptotic state of the autoionizing decay process. We would anticipate that this result is not unique to one-dimensional helium, but will apply in other systems as well, including real three-dimensional atomic systems. The decay rate of our chosen autoionizing state is 0.05 a.u.

We have examined the dipole matrix elements coupling the first excited bound state to the single-ionization continuum, and we have concluded that the lowest-energy autoionizing resonance is well described by the Fano formalism [8]. Because of the magnitude of the q parameter, no Fano minimum is apparent in the dipole matrix element at energies near the lowest autoionizing resonance.

ACKNOWLEDGMENTS

We acknowledge discussions with K. C. Kulander. This work was supported by the National Science Foundation through Grant No. PHY-9111562 to the University of Rochester and Grant No. PHY-9019783 to Calvin College. We also acknowledge assistance with computing resources from the Pittsburgh Supercomputing Center.

[1] L. V. Keldysh, Zh. Eksp. Teor. Fiz. **47**, 1945 (1964) [Sov. Phys. JETP **20**, 1307 (1965)].

[2] See, for example, M. V. Ammosov, N. B. Delone, and V. P. Krainov, Zh. Eksp. Teor. Fiz. **91**, 2008 (1986) [Sov. Phys. JETP **64**, 1191 (1986)].

[3] A number of experimental comparisons with the theory of Ref. [2] are available: S. Augst, D. Strickland, D. D. Meyerhofer, S. L. Chin, and J. H. Eberly, Phys. Rev. Lett. **63**, 2212 (1989); S. L. Chin, W. Xiong, and P. Lavigne, J. Opt. Soc. Am. B **4**, 853 (1987); B. Walker, E. Mevel, B. Yang, P. Breger, J. P. Chambaret, A. Antonetti, L. F. DiMauro, and P. Agostini, Phys. Rev. A **48**, R894 (1993).

[4] For an overview, see J. H. Eberly, R. Grobe, C. K. Law, and Q. Su, in *Atoms in Intense Laser Fields*, edited by M. Gavrila (Academic, Orlando, 1992).

[5] See K. C. Kulander, K. J. Schafer, and J. L. Krause, in *Atoms in Intense Laser Fields* (Ref. [4]).

[6] R. Grobe and J. H. Eberly, Phys. Rev. Lett. **68**, 2905 (1992); Phys. Rev. A **47**, R1605 (1993); **48**, 623 (1993); Laser Phys. **3**, 323 (1993).

[7] R. Grobe and J. H. Eberly, Phys. Rev. A **48**, 4664 (1993).

[8] U. Fano, Phys. Rev. **124**, 1866 (1961).

[9] A ground-state plot for a similar potential has been presented in M. S. Pindzola, D. C. Griffin, and C. Bottcher, Phys. Rev. Lett. **66**, 2305 (1991). Their Hamiltonian differs significantly from ours, however, in that theirs is invariant under all of the replacements $(x_1,x_2)\rightarrow(x_1,-x_2)\rightarrow(-x_1,x_2)$.

[10] R. Grobe, K. Rzazewski, and J. H. Eberly (unpublished).

[11] Hartree-Fock techniques are discussed in, for example, C. Froese Fischer, *The Hartree-Fock Method for Atoms* (Wiley, New York, 1977); R. D. Cowan, *The Theory of Atomic Structure and Spectra* (University of California Press, Berkeley, CA, 1981).

[12] Random-dot stereograms are discussed in A. A. Kinsman, *Random Dot Stereograms,* 1992 (available from Kinsman Physics, P. O. Box 22682, Rochester, NY 14692).

[13] P. E. Coleman and P. L. Knight, J. Phys. B **14**, 2139 (1981).

[14] A similar calculation using the He^+ basis states and the autoionizing state $|+a\rangle$ gives $q=-19$.

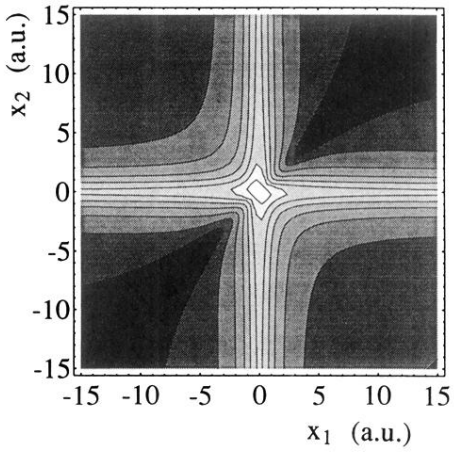

FIG. 1. Contour plot of the potential of Eq. (2) for $Z=2$. In this plot the shading darkens with increasing height.

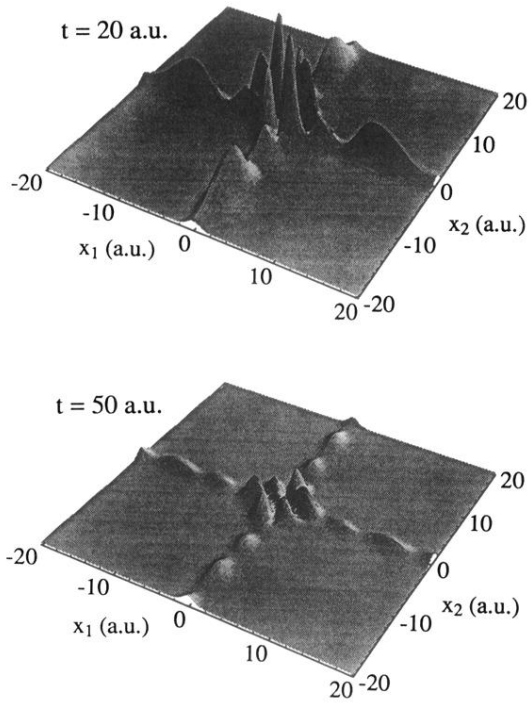

FIG. 10. Three-dimensional plots similar to Fig. 7, but for times $t=20$ and 50 a.u. The vertical scales are consistent for the two times, but both the vertical and spatial scales are changed from Fig. 7.

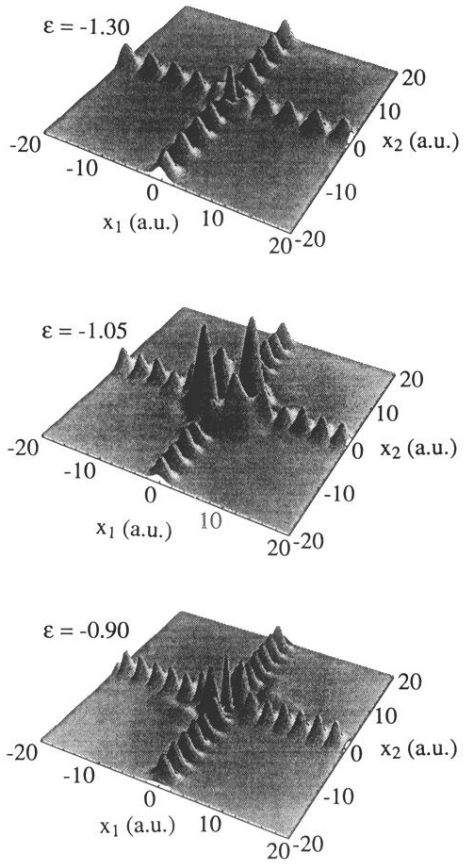

FIG. 5. Square of the continuum wave functions, $\langle x_1 x_2 | \varepsilon \rangle^2$, for energies $\varepsilon = -1.30$, -1.05, and -0.90. The three plots have the same vertical scale.

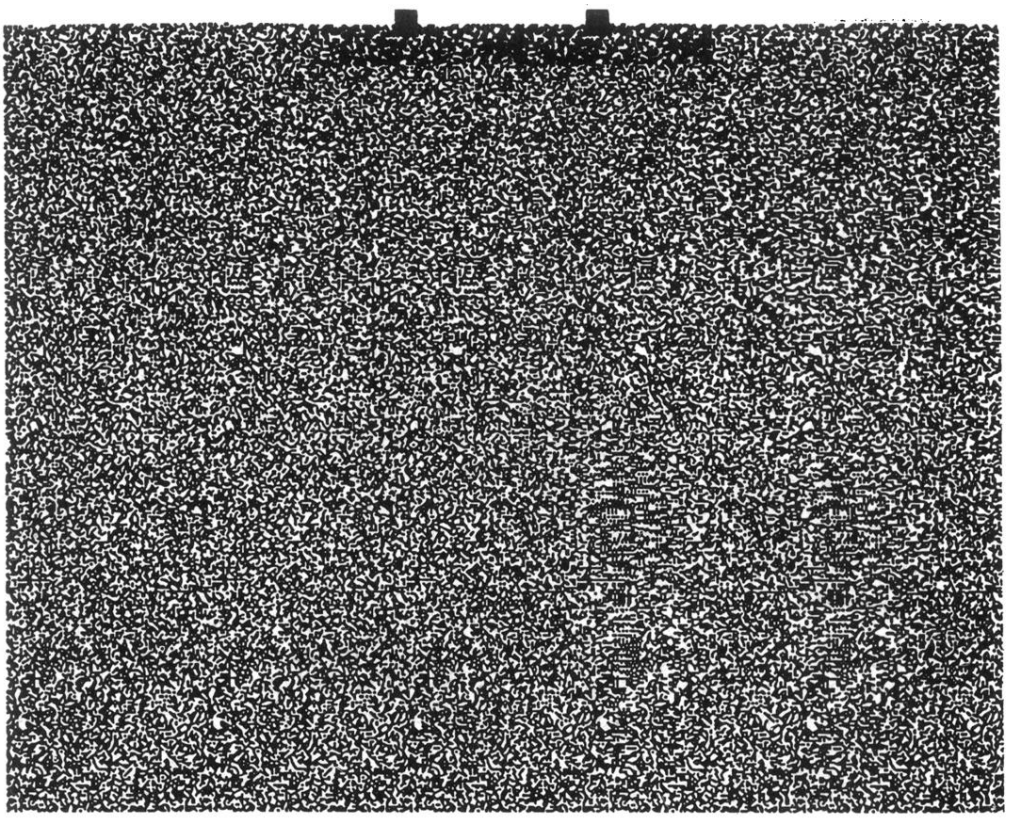

FIG. 6. Three-dimensional image of the spatial wave function of $|a\rangle$ vs x_1 and x_2, seen directly from above. To see the image, one should focus one's eyes *behind* the plane of the page in such a way that the two large black spots near the top center of the field are seen as three (not two or four) spots. This can often be done by first holding the page near one's face with the eyes relaxed and then slowly moving the page outward while watching the large spots [12]. A plot of the square of the wave function is shown in the top row of Fig. 7.

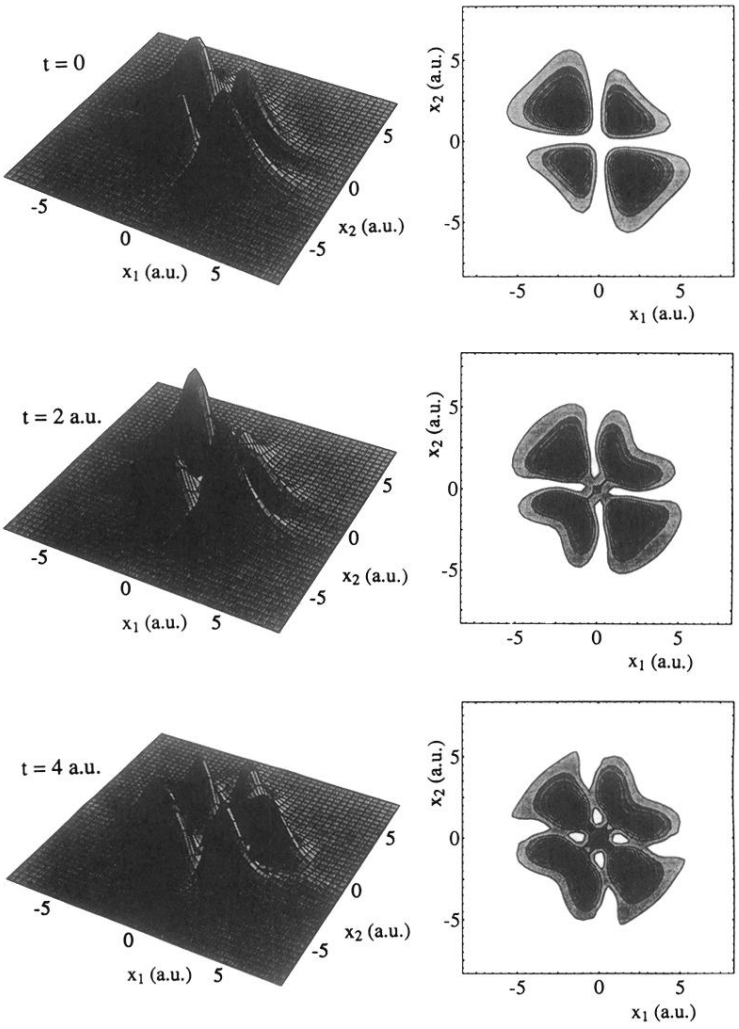

FIG. 7. Three-dimensional and contour plots of the two-electron probability $|\Psi(x_1,x_2;t)|^2$ as a function of the electron coordinates x_1 and x_2 at time $t=0$, 2, and 4 a.u. The vertical scaling and contour levels are consistent for the different times.

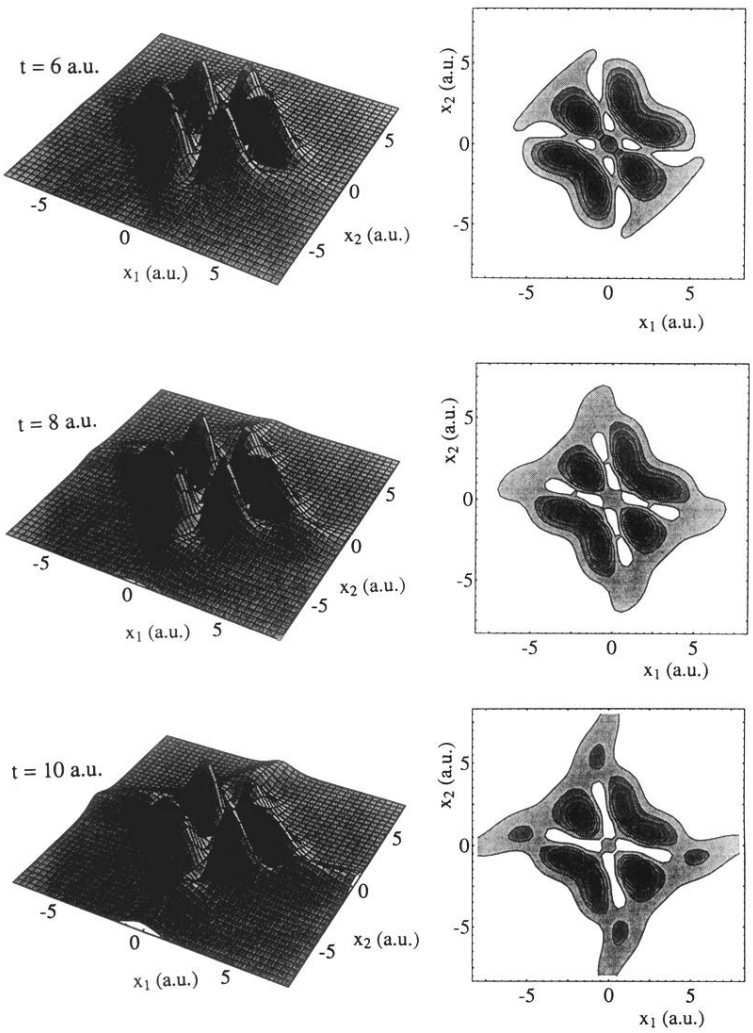

FIG. 8. Similar to Fig. 7, but at times $t=6$, 8, and 10 a.u. Scales are the same as in Fig. 7.